Electronic Supplementary Material (ESI) for Journal of Materials Chemistry A.

Supplementary Information

Integrated Organic–Inorganic Hole Transport Layer For Efficient and Stable Perovskite Solar Cells

Yaxiong Guo[a], Hongwei Lei[b], Liangbin Xiong[c], Borui Li[a], Guojia Fang[a]*

[a] *Key Lab of Artificial Micro- and Nano-Structures of Ministry of Education of China, School of Physics and Technology, Wuhan University, Wuhan 430072, P. R. China. *E-mail: gjfang@whu.edu.cn*

[b] *Department of physics, College of Science, Central China Agricultural University, Wuhan 430070, P. R. China.*

[c] *School of Physics and Electronic-information Engineering, Hubei Engineering University, Xiaogan, 432000, P. R. China.*

Experimental Section

Device Fabrication:

FTO glasses were cleaned with detergent, deionized water and acetone and sonicated with ethanol in an ultrasonic bath for 10 min. UVO was treated for 15 min prior to use. SnO_2 electron transporting layer (ETL) was deposited following our previous work. Typically, 0.1 M $SnCl_2 \cdot 2H_2O$ solution dissolved in ethanol was spin-coated on FTO substrate at 2000 rpm for 40 s. To form dense ETL, the substrates were annealed at 180 °C in air for 1 h. Afterwards 15 mg ml^{-1} of PCBM solution was spin-casted at 3000 rpm for 40 s on SnO_2 ETL to passivate the interface. Then, 461 mg of PbI2 (TCI) and 159 mg of CH_3NH_3I and were dissolved in 723 μl of N, N-dimethylformamide (DMF) and 81 μl dimethyl sulfoxide (DMSO). The mixed solution was stirred at 70°C for 10 h before using. Subsequently, perovskite film was formed by spin-casting the solution on FTO/SnO_2/PCBM substrate at 4000 rpm for 30 s. note that 300 μL chlorobenzene was dripped on the rotating substrate to aid the formation of uniform, dense and crystalline perovskite film. Then, the film was thermally annealed at 60°C for 2 min and 100 °C for 5 min. After the deposition of perovskite materials, spiro-OMeTAD (70 mM in chlorobenzene) was spin-coated on the perovskite layer at 3000 rpm for 30 s. This solution was doped with 29 μL of tBP and 17.5 μL of Li-TFSI (520 mg mL^{-1} in acetonitrile). For the samples with hybrid bilayer HTL, FBT-Th4 solution (5 mg in chlorobenzene) was spin-coated on the perovskite layer at 2000 rpm for 30 s, and then annealed at 85°C for 5 min, inorganic Cu_xO HTL was prepared on top of FBT-Th4 by vacuum thermal evaporation of Cu_2O powder (Aldrich, 99.99%). Finally, the electrode was deposited by thermal evaporation of gold under a pressure of 5×10^{-5} Torr. The active area was 0.09 cm^2 defined by the shadow mask.

Material and device characterization:

The crystal structure of the Cu_xO and perovskite films were characterized by X-ray diffraction (XRD). Conventional XRD in Bragg-Brentano configuration has been performed by the same Bruker D8 Advance diffraction meter using Cu Kα radiation at 40 kV and 40 mA. Line traces were collected over 2θ values ranging from 10° to 80°. The transmittance of the films was measured by a UV-VIS-NIR spectrophotometer (CARY5000, Varian) in the 300-800 nm wavelength range at RT. The surface morphologies were made in a scanning electron microscope (SEM, FEI XL-30). Transmission electron microscopy (TEM) characterization was carried out using JEOL JEM 2010. X-ray photoelectron spectroscopy (XPS) and ultraviolet photoelectron spectroscopy (UPS) were performed using a XPS/UPS system (Thermo Scientific, ESCLAB 250Xi, USA). The compositions and chemical states of Cu_xO film were examined by XPS. Before been tested, samples were sputtering-cleaned by the lower energy of Ar^+ to remove atmospheric contamination in the XPS chamber for approximately 30 s, and the Ar^+ gun was operated at 0.5 kV at a pressure of 1×10^{-7} Pa. The vacuum pressure of the analysis chamber was better than 1×10^{-8} Pa. The whole survey scan to identify the overall surface composition and chemical states were performed, using a monochromated Al Ka X-ray source (=1486.68 eV), detecting photoelectrons at a 150 eV pass energy and a channel width of 500 meV. The surface carbon signal at 284.6 eV was used as an internal standard. The work function and band energy position were calculated by UPS. UPS was carried out using Helium I α radiation from a discharge lamp operated at 90 W, a pass energy of 10 eV, and a channel width of 25 meV. A −9 V bias was applied to the samples, in order to separate the sample and analyze low-kinetic-energy cutoffs. The morphologies of perovskite and different HTLs spin-casted on perovskite were characterized by atomic force microscopy (AFM, SPM-9500J3, Shimadzu, Japan). The photoluminescence (PL) measurements were carried out under a 488 nm laser at RT and the emissions were collected via a HORIBA Jobin-Yvon monochromator. The current-voltage (*J*-*V*) curves of the devices were obtained using a computer-controlled Keithley 2400 Source Measure Unit and the device test was carried out under illumination of AM 1.5G, 100 mW cm^{-2} (the light intensity was calibrated using a Si photodiode) at RT using a solar simulator. The corresponding incident photon-to-electron conversion efficiency (IPCE) spectrum was measured with a QE/IPCE measurement system (Enli Technology Co. Ltd). SCLC measurement were conducted by fabricating devices with structures of FTO/PEDOT:PSS/FBT-Th4/Cu_xO/Au or FTO/PEDOT:PSS/spiro-OMeTAD/Au and then testing the *J-V* curves of the devices using the Keithley 2400 Source Measure Unit. Hole mobility was extracted by fitting the *J-V* curves according to the modified Mott-Gurney equation: $J = \frac{9}{8}\varepsilon_r\varepsilon_0\mu_{h(e)}\frac{V^2}{L^3}$ In the equation, ε_0 is the permittivity of free space, ε_r is the permittivity of the polymer, $\mu_{h(e)}$ is the carrier mobility, and *L* is the thickness of the active layer. The dielectric constant ε_r is assumed to be ~28, which is a typical value for conjugated polymers. For heterojunction solar cells calculation, a diode model can be used to analyze the *J-V* curve, from which we can get the series resistance (R_s) according to the linear fit of the data. $-\frac{dV}{dJ} = \frac{AK_BT}{e}\left(J_{SC} - J\right)^{-1} + R_S$ A is the ideality factor of the heterojunction, K_B is the Boltzmann constant, T is the absolute temperature and e is the elementary charge. For TRPL measurements, samples were excited with a 532 nm pulsed laser (pulse width ≈ 5 ps, beam diameter ≈ 150 μm) at 1.5×10^{10} photons $pulse^{-1}$ cm^{-2}. TRPL was performed with time correlated single photon counting (TCSPC) module (Becker & Hickel Simple Tau SPCM 130-E/M module) and the PL signal was collected (Integration time = 500 s) via hybrid APD/PMT module (R10467U-50). The TPV and TPC measurements are performed under dark condition, excited by a 532 nm pulse laser with certain intensity.

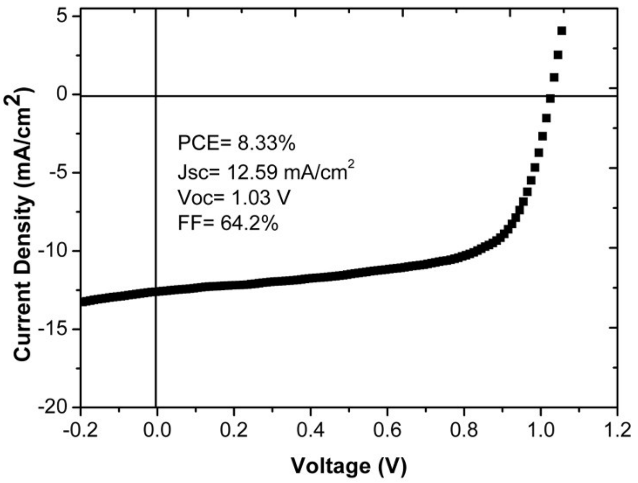

Figure S1. Typical *J*-*V* curves of the planar perovskite photovoltaic devices based on Cu_xO.

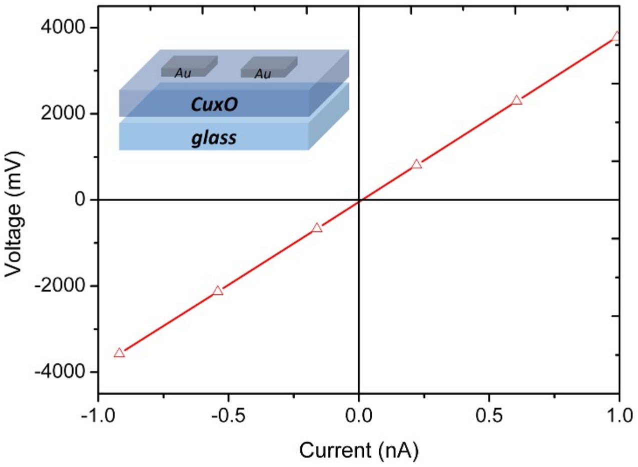

Figure S2. Typical contact *I*-*V* curve of the glass/Cu_xO/Au device. *I*-*V* curve shows a linear relationship, suggesting a good Ohmic contact between Au and Cu_xO. Cu_xO and top electrode Au were evaporated on glass substrate sequentially.

Table S1. Optical and electrochemical properties of FBT-Th4.

Compound	$\lambda_{Abs,max}{}^{a}$ (solution) (nm)	$\lambda_{Abs,max}$ (film) (nm)	Eg_{opt} (eV)	$Eg_{CV}{}^{a}$ (eV)	$HOMO_{CV}{}^{a}$ (eV)	$LUMO_{CV}{}^{a}$ (eV)	$HOMO_{UPS}$ (eV)	$LUMO_{UPS}$ (eV)
FBT-Th4	702	701	1.66	1.62	-5.36	-3.74	-5.34	-3.68

[a] the data are reported in literature.[1, 2]

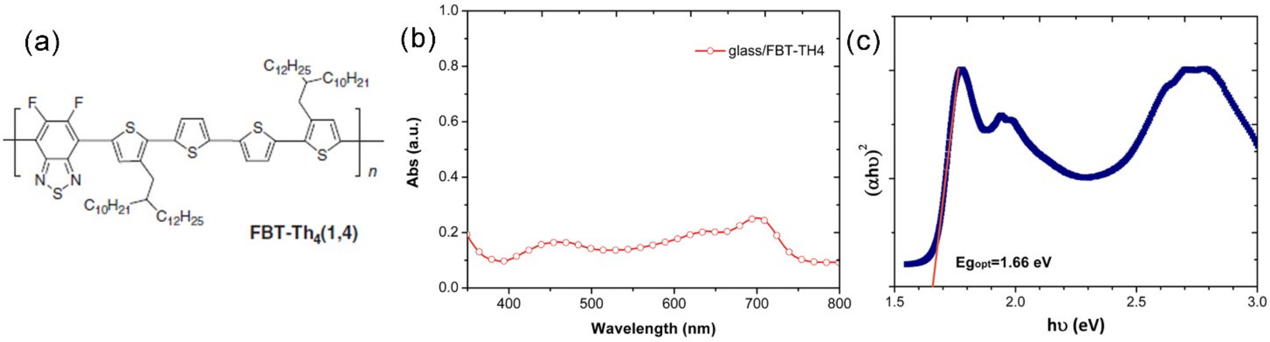

Figure S3. Molecular structure of the FBT-Th4 and UV-vis absorption spectra of the pristine FBT-Th4 film on a quartz glass substrate and optical band gap was calculated from the onset of absorption.

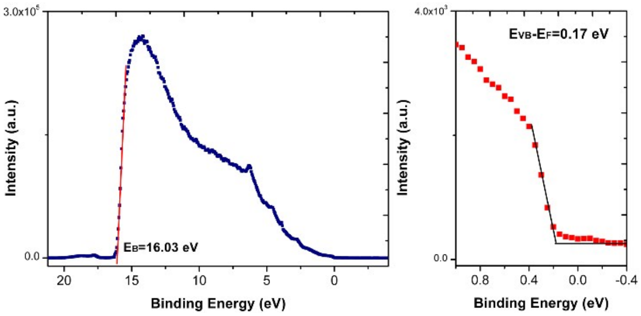

Figure S4. UPS spectra of FBT-Th4 film.

Solar cell characterization.

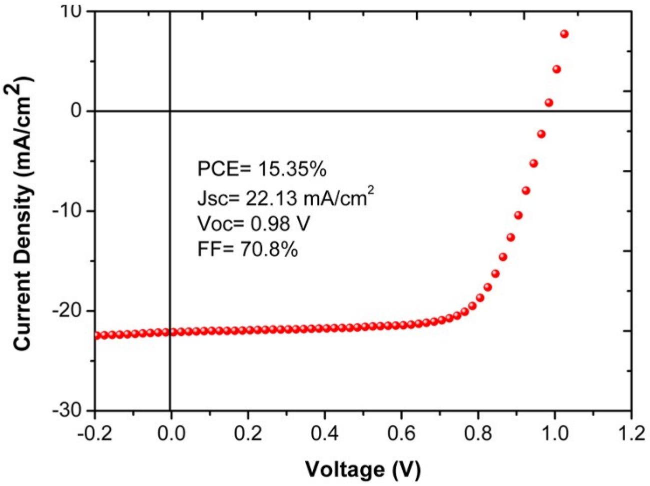

Figure S5. Typical *J-V* curves of the planar perovskite photovoltaic devices based on FBT-Th4 HTM.

Table S2. Figures of merit for a complete solar cell and solar cells missing either the Cu_xO or the FBT-Th4 polymer layer.

Device Structure	J_{SC} ($mA\cdot cm^{-2}$)	V_{OC} (V)	FF (%)	PCE (%)
$FTO/SnO_2/MAPbI_3/Cu_xO/Au$	12.59	1.03	64.2	8.33
$FTO/SnO_2/MAPbI_3$/FBT-Th4/Au	22.13	0.98	70.8	15.35

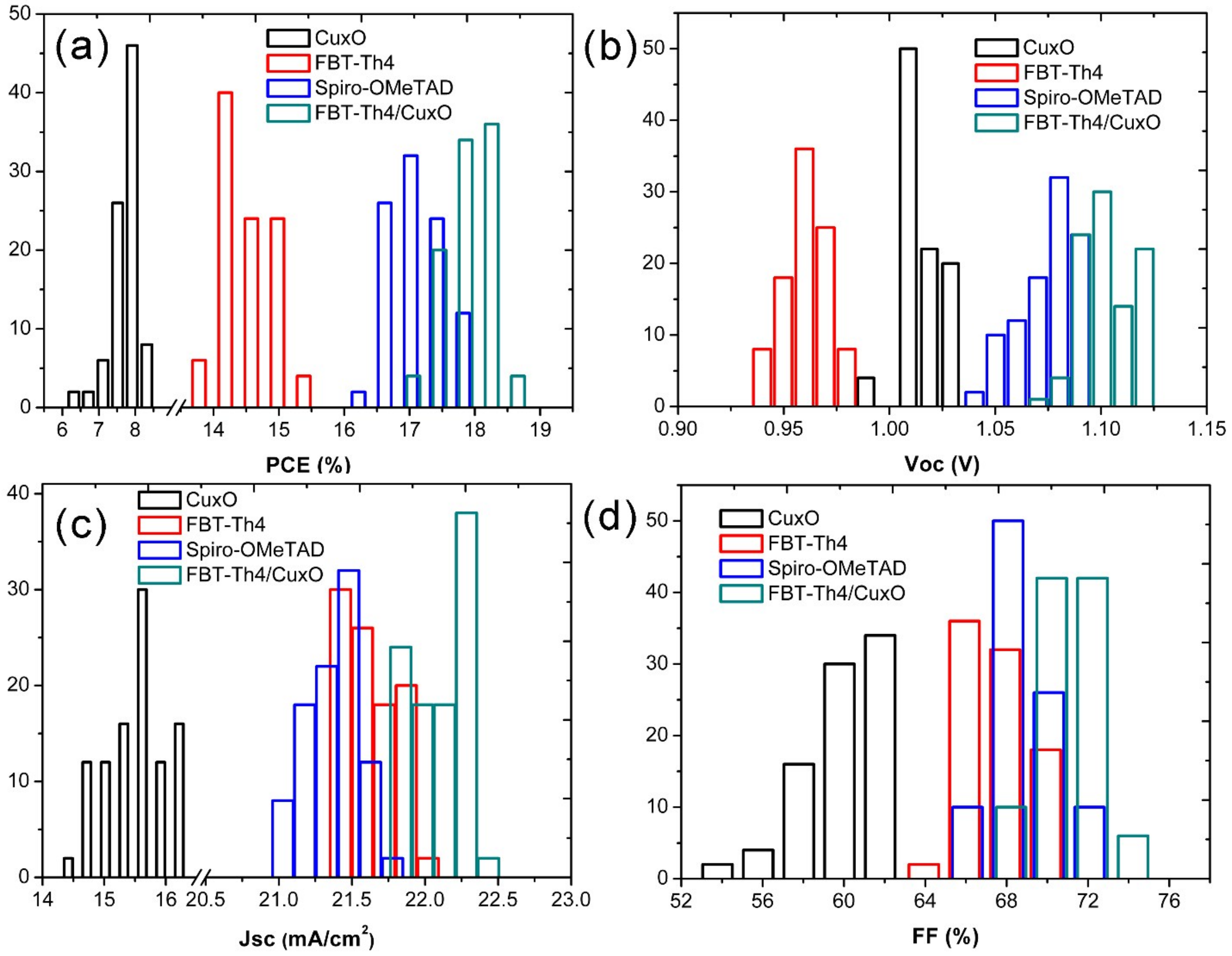

Figure S6. Statistics of device performance parameters (a) PCE, (b) V_{OC}, (c) J_{SC}, and (d) FF of the $MAPbI_3$ perovskite solar cells based on different HTMs.

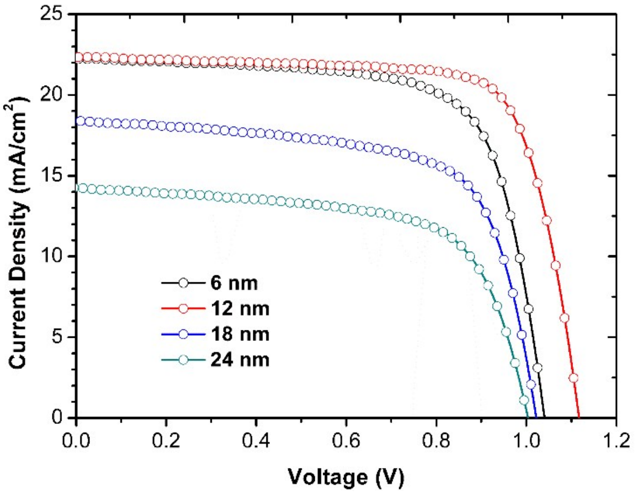

Figure S7. Typical *J-V* curves of the planar perovskite photovoltaic devices based on FBT-Th4/Cu$_x$O hybrid HTM with varied Cu$_x$O thickness of 6 nm, 12 nm, 18 nm and 24 nm.

Table S3. Summary of PCE performances of planar devices based on hybrid HTM with varying thicknesses of Cu$_x$O obtained from Figure S6.

Cu$_x$O thickness (nm)	J_{SC} (mA·cm^2)	V_{OC} (V)	FF (%)	PCE (%)
6 nm	22.22	1.040	71.1	16.44
12 nm	22.34	1.120	75.4	18.85
18 nm	18.38	1.025	67.4	12.70
24 nm	14.24	1.000	65.6	9.37

Optoelectronic characterization.

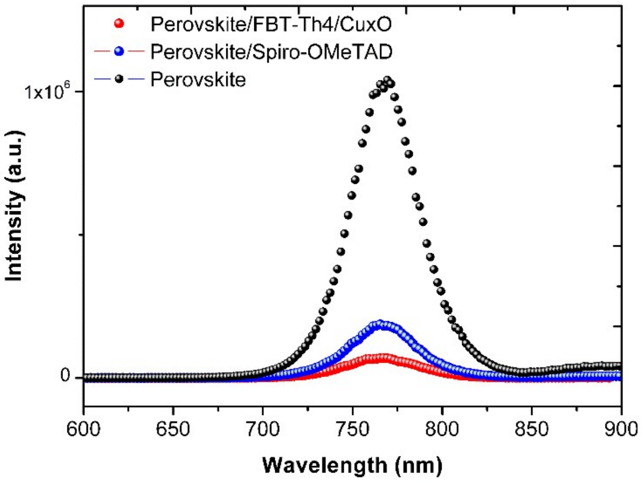

Figure S8. Steady-state PL spectra of the perovskite/spiro-OMeTAD, perovskite/FBT-Th4/Cu$_x$O and bare perovskite film.

Table S4. Fitting parameters of bi-exponential decay function in time-resolved PL spectra.

Films	A_1	τ_1 (ns)	A_2	τ_2 (ns)	Average decay time τ (ns)[a]
Perovskite	2031.3	65.4	1688.8	20.7	45.1
Perovskite/spiro-OMeTAD	770	6.5	310.8	42.9	16.9
Perovskite/FBT-Th4/Cu$_x$O	872.6	7.8	279.3	27.0	12.4

[a] Average decay time is calculated according to the equation: $\tau = (A_1\tau_1 + A_2\tau_2)/(A_1 + A_2)$.

Table S5. Fitting parameters of bi-exponential decay function in transient photovoltage measurement.

Films	A_1	τ_1 (ms)	A_2	τ_2 (ms)	Average decay time τ (ms)[a]
Perovskite/spiro-OMeTAD	0.45	0.02	0.36	0.20	0.09
Perovskite/FBT-Th4/Cu$_x$O	0.41	0.04	0.57	0.22	0.13

[a] Average decay time is calculated according to the equation: $\tau = (A_1\tau_1 + A_2\tau_2)/(A_1 + A_2)$.

Table S6. Fitting parameters of bi-exponential decay function in transient photocurrent measurement.

Films	A_1	τ_1 (μs)	A_2	τ_2 (μs)	Average decay time τ (μs)[a]
Perovskite/spiro-OMeTAD	0.86	0.52	0.86	0.52	0.52
Perovskite/FBT-Th4/Cu$_x$O	0.82	0.42	0.82	0.42	0.42

[a] Average decay time is calculated according to the equation: $\tau = (A_1\tau_1 + A_2\tau_2)/(A_1 + A_2)$.

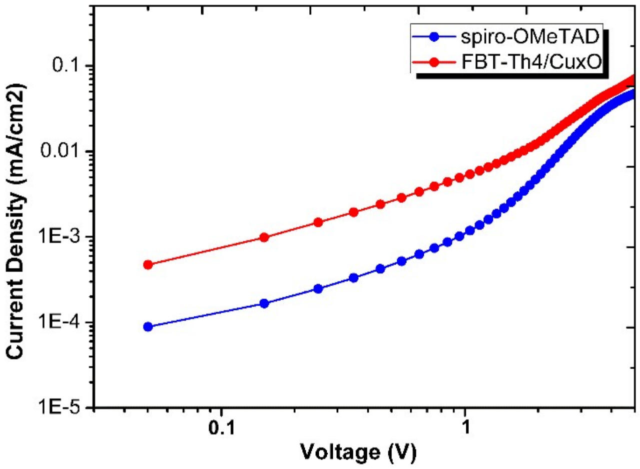

Figure S9. (a) J−V curves of the hole-only devices ITO/PEDOT:PSS/$MAPbI_3$/HTMs/Au.

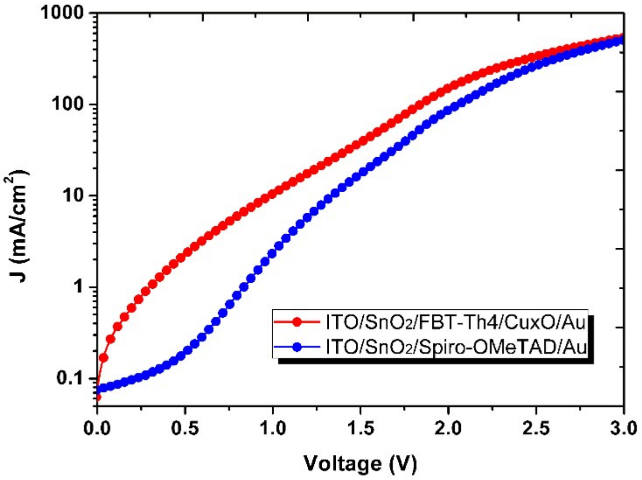

Figure S10. (b) Comparison of charge transport or injection properties from the devices using spiro-OMeTAD and FBT-Th4/Cu_xO, respectively.

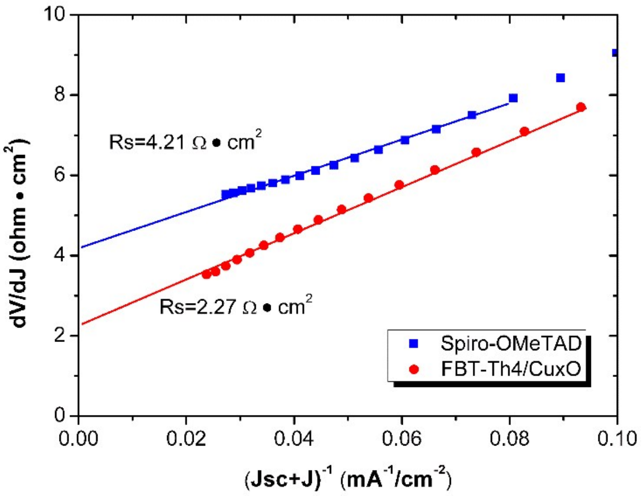

Figure S11. (c) Plots of -dV/dJ vs (J_{SC}-J)$^{-1}$ and the linear fitting curves.

Stability.

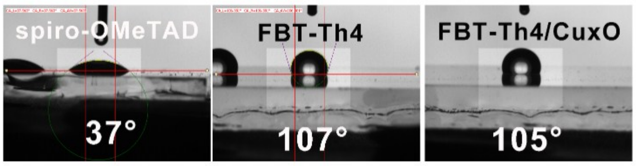

Figure S12. Contact angle measurements taken of water droplets on films of spiro-OMeTAD and FBT-Th4 and both FBT-Th4/Cu$_x$O complexes.

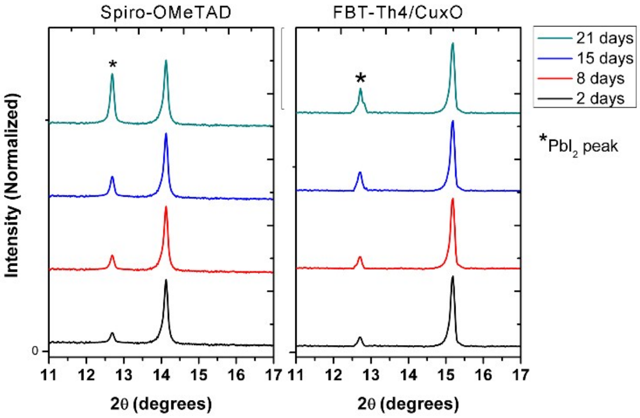

Figure S13. X-ray diffraction (XRD) measurements. a) XRD pattern of MAPbI$_3$ perovskite films with various HTMs, compared from freshly made to 21 days in ambient atmosphere in the dark.

HTMs	*Aging time* [hours]	*Voc* [V]	*Jsc* [mA cm^{-2}]	*FF* [%]	*PCE* [%]
FBT-Th4/ Cu$_x$O	0	1.12	22.3	75.4	18.85
	12	1.11	22.14	74.5	18.31
	24	1.115	22.05	73.3	18.03
	48	1.11	21.8	72.6	17.59
	72	1.1	21.905	72.5	17.47
	168	1.09	21.7	72.8	17.27
	240	1.085	22.1	72.5	17.39
	384	1.095	21.82	72.1	17.23
	504	1.09	22.12	71.5	17.24
Spiro-OMeTAD	0	1.105	21.78	72.2	17.38
	12	0.95	19.01	40.9	7.39
	24	0.925	19.31	43.5	7.77
	48	0.92	17.52	44.6	7.20
	72	0.91	18.02	46.2	7.58
	168	0.945	18.91	45.1	8.06
	240	0.96	17.62	48.8	8.25
	384	0.98	15.14	50.5	7.49
	504	0.99	12.27	48.2	5.85

Table S7. Performance of PSC stability for 500 h at 70%-80% humidity of nonencapsulated high-performance perovskite solar cells based on FBT-Th4/Cu$_x$O and spiro-OMeTAD.

Table S8. Initial steady-state efficiencies compared to steady-state efficiencies measured after 500 h at 70% humidity of non-encapsulated perovskite solar cells.

HTMs	PCE$_{\text{Initial}}$ [%]	PCE$_{\text{500h}}$ [%]	PCE$_{\text{500h}}$/PCE$_{\text{initial}}$ [%]
FBT-Th4/Cu$_x$O	18.85	17.24	91.4
Spiro-OMeTAD	17.38	5.85	33.6

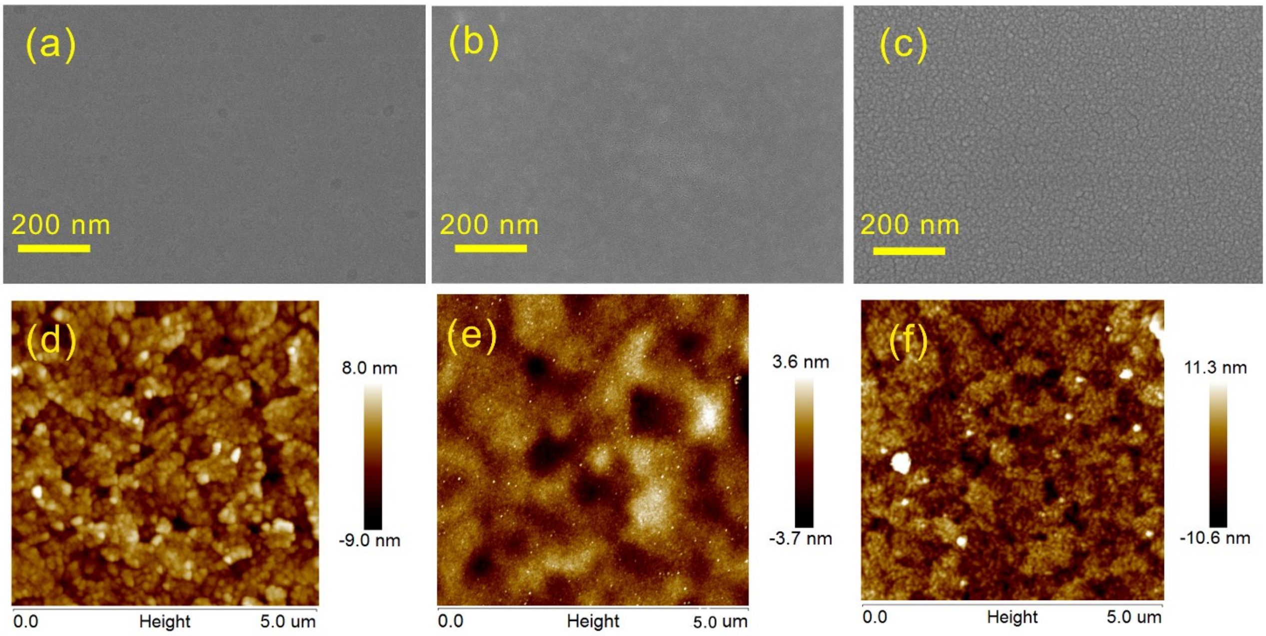

Figure S14. (a) SEM image of Spiro-OMeTAD film spin-casted on FTO/SnO_2/perovskite, (b) SEM image of FBT-Th4 film spin-casted on FTO/SnO_2/perovskite, (c) SEM image of Cu_xO film deposited on FTO/SnO_2/perovskite/FBT-Th4. The corresponding AFM images of (d) Spiro-OMeTAD film on FTO/SnO_2/perovskite, (e) FBT-Th4 film on FTO/SnO_2/perovskite and (f) Cu_xO film on FTO/SnO_2/perovskite/FBT-Th4.

References

1. Z. Chen, P. Cai, J. Chen, X. Liu, L. Zhang, L. Lan, J. Peng, Y. Ma and Y. Cao, *Advanced materials*, 2014, 26, 2586-2591.
2. M. Li, C. An, T. Marszalek, M. Baumgarten, K. Mullen and W. Pisula, *Advanced materials*, 2016, 28, 2245-2252.